SiliconPV 2025, 15th International Conference on Crystalline Silicon Photovoltaics

Advances in Industrial Silicon Solar Cells

https://doi.org/10.52825/siliconpv.v3i.2708

Published: 27 Jan. 2026

Development of a p-type Silicon Interdigitated Back Contact Solar Cell With Passivated Contacts

Lazhar Rachdi[1,*], Marius Meßmer[2], Mertcan Comak[1], Jan Lossen[1], Andreas Wolf[2], and Lejo Joseph Koduvelikulathu[1]

[1]International Solar Energy Research Center (ISC) Konstanz, Germany

[2]Fraunhofer Institute for Solar Energy Systems (ISE), Germany

*Correspondence: Lazhar Rachdi, lazhar.rachdi@isc-konstanz.de

Abstract. P-type interdigitated back contact (pIBC) solar cells represent a promising alternative to the currently dominant Tunnel Oxide Passivated Contact (TOPCon) technology, utilizing the industrially established metallization scheme of Passivated Emitter and Rear Cells (PERC) for the p-type base while incorporating TOPCon metallization for the n-type polycrystalline emitter. In this study, we present the results of optimization efforts aimed at increasing the efficiency pIBC cells manufactured in our lab by minimizing metallization-induced losses. Aluminum pastes with varying silicon content were used, and the firing temperature was adjusted. These modifications resulted in a reduction in the metallization-induced Voc loss after aluminum metallization to 5 mV, along with contact resistance values below 1 mΩ.cm². Additionally, reducing the n-polySi thickness led to a decrease in free carrier absorption and an increase in Jsc. Finally, we achieved non-metallized cell precursors exhibiting iVoc values between 730 and 740 mV and a champion solar cell efficiency of 23.3%.

Keywords: IBC, P-Type, TOPCon, Passivated Contact

1. Introduction

Passivated Emitter and Rear Cell (PERC) technology has been dominating the market since years and is expected to slowly fade as TOPCon (Tunnel Oxide Passivated Contact) emerges to take its place [1]. An interesting option for the remaining PERC lines is to convert them directly into p-type interdigitated back contact (pIBC) solar cells. This technology offers a high tool reutilization, facilitating a smoother transition while maximizing the use of existing equipment. pIBC technology offers several compelling advantages over TOPCon, including reduced reliance on silver paste, which could significantly decrease silver consumption [2]. Additionally, pIBC has a relatively low thermal budget compared to the energy-intensive boron diffusion used in standard TOPCon processes.

In this study, we present our advances in the development of a pIBC solar cell on p-type Ga-doped mono Cz-substrates. A Quokka3 [3] simulation (not shown here) identified aluminum metallization as the key efficiency bottleneck, affecting both the V_{oc} and *FF*. We investigated the effect of the silicon content in the aluminum paste on V_{oc} loss and contact resistance. Moreover, we studied the effect of depositing thinner n-polySi layers to reduce parasitic light absorption.

2. Samples preparation

The experiments are conducted on commercial M2-sized Ga-doped p-type Cz-Si wafers with resistivities ranging from 1 to 2 Ω.cm. The p-type wafers undergo an alkaline single-side texturing procedure in order to obtain random pyramids on the front side and a polished surface on the rear side. This step is achieved by means of PECVD SiO_x masking on the front side of the wafer to protect the texturing during subsequent KOH etching. It is followed by a wet-chemical cleaning process. Subsequently, a thin interfacial oxide layer is thermally grown in a tube furnace, and an in-situ phosphorus-doped a-Si(n) layer is deposited on the rear side using PECVD with silane (SiH_4) and phosphine (PH_3) as reactive gases. The wafers are then subjected to thermal annealing/oxidation using O_2 as the processing gas, which serves as the n-polySi crystallization step and simultaneously forms a front-side protective mask layer.

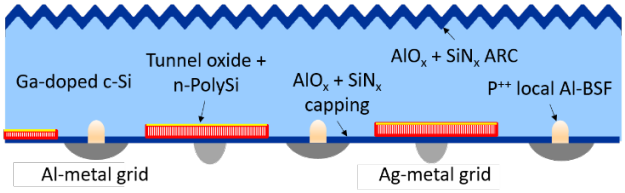

Figure 1. *Schematic cross section of the p-IBC solar cell*

The interdigitated base and emitter region pattern is defined using laser ablation with a nanosecond green laser, followed by wet-chemical alkaline removal of laser-induced damage and an oxidative wet-chemical cleaning. A passivation stack of AlO_x/SiN_y is deposited on both sides via ALD and PECVD. The ALD process consists of alternating cycles in a process tube, in which the O_2 is dissociated during the first step by plasma generated with an RF source, and a TMA step is conducted thermally at approximately 300°C. Laser contact opening (LCO) of the passivation stack in the base region is carried out by a nanosecond green laser, and subsequently, aluminum base contacts are printed, similar to the PERC process base contact formation. Silver contacts are established on the n-polySi emitter region using screen printing, followed by a standard co-firing process at a peak temperature of about 800°C. A schematic cross-section of the finalized solar cell is shown in Figure 1.

3. Results

3.1 Printing and firing optimization

To minimize contact recombination and resistance caused by the base region metallization, aluminium pastes with varying silicon content were studied. The contact resistance was evaluated on dedicated test structures using the transfer length method (TLM). The iV_{oc} loss was determined using PL image processing. Because QSSPC cannot be performed on metallized areas, the area-averaged PL intensity from non-metallized regions was first converted to iV_{oc} using QSSPC as a calibration reference. This calibration was then applied to the PL images of the metallized areas to calculate their area-averaged iV_{oc}. Finally, the iV_{oc} from metallized areas was subtracted from the iV_{oc} of the non-metallized areas to obtain the iV_{oc} loss within the same wafer (examples shown in Figure 4).

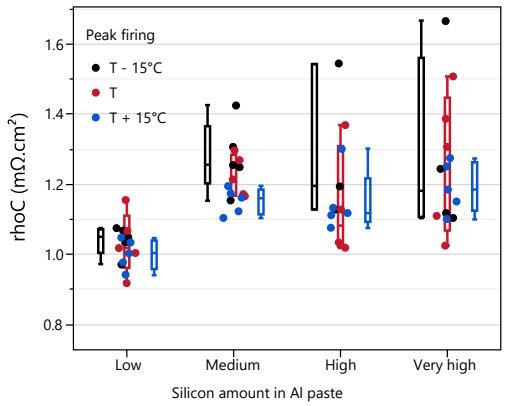

Figure 2. *Contact resistance obtained by TLM. Al pastes with different Si content and firing temperatures were investigated*

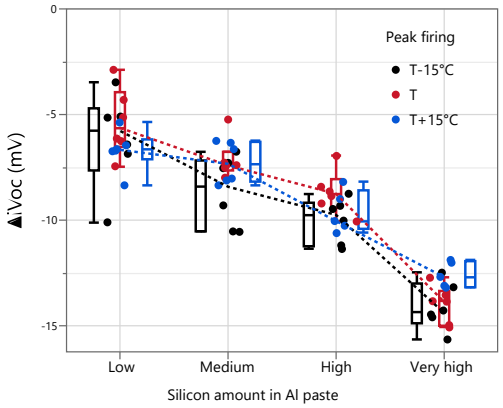

Figure 3. *iV_{oc} loss after metallization. Al pastes with different Si content and firing temperatures were investigated*

Figure 2 shows the dependence of the contact resistance as function of the silicon content in the Al paste. A trend of increasing contact resistance with higher silicon content and lower peak temperature was observed. Promising values < 1 mΩ.cm² could be obtained with low silicon-containing Al pastes, while simultaneously expanding the firing window possibilities.

Figure 3 shows the impact of the silicon amount in the aluminium paste on the PL calculated iV_{oc} loss after metallization. It is interesting to notice that lower silicon content favors lower metallization losses as opposed to previous investigations [4], [5]. Fine tuning the peak firing temperature allowed us to reduce the iV_{oc} loss to about 5 mV.

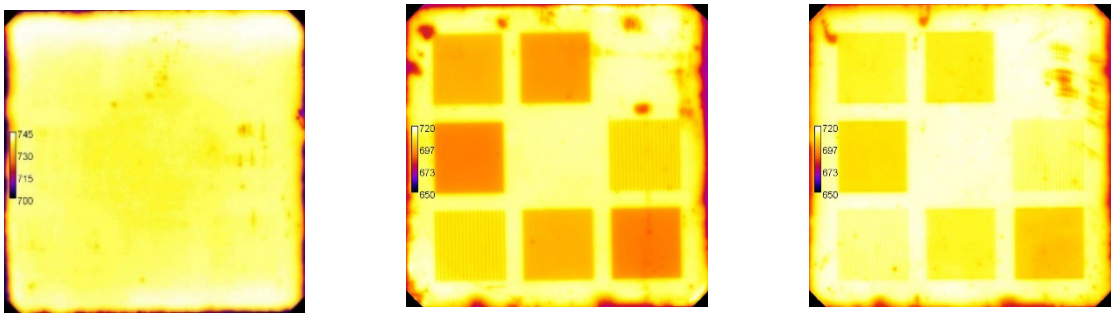

Figure 4*. PL images depicting metallized $J_{o,met}$ symmetrical samples with varying metallization density on n-polySi (left), p-type base before optimization (middle) and p-type base after optimization (right)*

Figure 4 shows exemplary PL images of partially metallized test samples (with different metallization fractions) used to evaluate the iV_{oc} to V_{oc} loss. In the left PL image, the vanishing metallization on the n-polySi wafers (using silver paste) is a strong indication of well-passivated contacts. The middle and right PL images depict the metallized base region with aluminum paste before and after optimization, respectively. It is evident that the metallized region exhibits higher PL intensity after paste and firing optimization.

3.2 n-polySi Thickness optimization

Further process optimization is carried out on the rear side of the cell by varying the n-polySi thickness. Figure 5 shows the effect of this variation on the cell characteristics

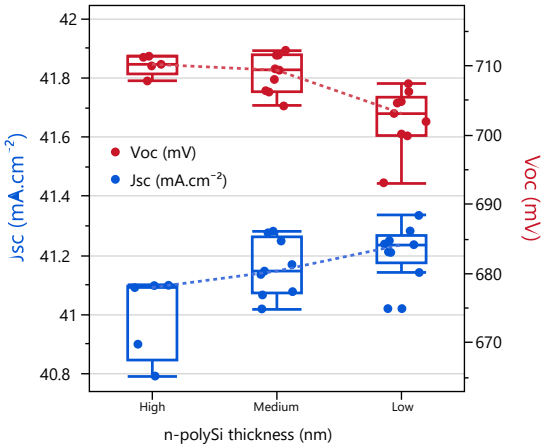

Figure 5. *J_{sc} and V_{oc} of pIBC solar cells obtained by IV-measurements as function of the n-polySi thickness*

Figure 5 shows that by decreasing the n-polySi thickness, a gain of 0.1 mA·cm⁻² in J_{sc} can be achieved due to reduced free carrier absorption. However, the V_{oc} was negatively impacted by this change. Further studies are needed to determine whether this decrease can be correlated with the metallization, in particular with paste penetration through the tunnel oxide [6].

3.3 Solar cell results

After implementing the learnings from a series of optimization procedures, the implied open-circuit voltage (iV_{oc}) and the current-voltage (IV) characteristics of our best-performing solar cell batch are depicted in Figure 6 and 7, respectively.

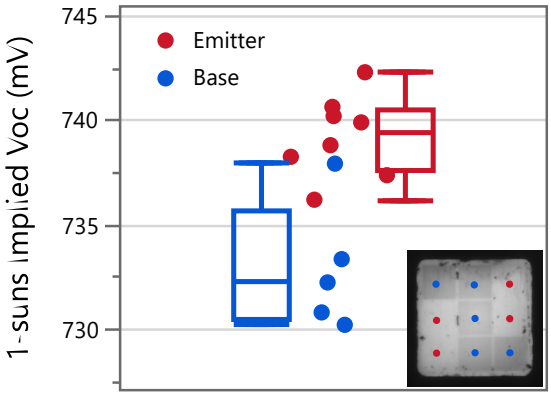

Figure 6*. iV_{oc} results of non-metallized test fields on specifically created structures (shown in the PL image in the corner)*

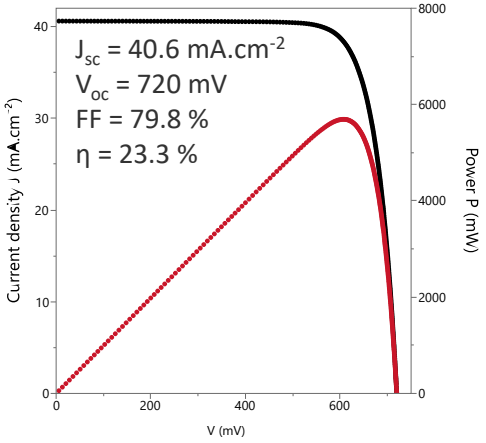

Figure 7*. IV curves and characteristics of our current champion pIBC cell*

Figure 6 shows the lifetime results of asymmetrical test structures designed to replicate our solar cell, where large laser-ablated fields were used instead of the usual IBC stripe ablation to enable QSSPC measurements. The non-metallized test fields achieve a promising iV_{oc} of 733 mV on the base region and 740 mV on the n-polySi region. The champion solar cell reaches an efficiency of 23.3%. We are planning further optimization with the goal of increasing efficiency [7].

Data availability statement

The data that support the findings of this study are available from the corresponding author upon reasonable request.

Author contributions

L. Rachdi: Conceptualization, investigation, visualization, writing – original draft

M. Meßmer: Conceptualization, investigation, review

M. Comak: Investigation, review

J. Lossen: Supervision, project administration, review

A. Wolf: Conceptualization, review

L.J. Koduvelikulathu: Supervision, project administration, review

Competing interests

The authors declare that they have no competing interests.

Funding

The authors would like to acknowledge financial support by the German Federal Ministry of Economic Affairs and Climate Action within the research projects “OLIVIA” (contract number 03EE1184E).

References

[1] M. Fischer, M. Woodhouse, and P. Baliozian, “International Technology Roadmap for Photovoltaic (ITRPV) 2023 Results.” Accessed: Oct. 23, 2024. [Online]. Available: https://www.vdma.org/international-technology-roadmap-photovoltaic

[2] B. Kafle, B. S. Goraya, S. Mack, F. Feldmann, S. Nold, and J. Rentsch, “TOPCon – Technology options for cost efficient industrial manufacturing,” *Solar Energy Materials and Solar Cells*, vol. 227, p. 111100, Aug. 2021, doi: 10.1016/j.solmat.2021.111100.

[3] A. Fell, “A Free and Fast Three-Dimensional/Two-Dimensional Solar Cell Simulator Featuring Conductive Boundary and Quasi-Neutrality Approximations,” *IEEE Transactions on Electron Devices*, vol. 60, no. 2, pp. 733–738, Feb. 2013, doi: 10.1109/TED.2012.2231415.

[4] M. Rauer *et al.*, “Investigation of Aluminum-Alloyed Local Contacts for Rear Surface-Passivated Silicon Solar Cells,” *IEEE Journal of Photovoltaics*, vol. 1, no. 1, pp. 22–28, Jul. 2011, doi: 10.1109/JPHOTOV.2011.2161864.

[5] Z.-W. Peng, M. Nakahara, T. Buck, and R. Kopecek, “Investigation on Industrial Screen-Printed Aluminum Point Contact and Its Application in n-PERT Rear Junction Solar Cells,” *IEEE Journal of Photovoltaics*, vol. 9, no. 6, pp. 1554–1562, Nov. 2019, doi: 10.1109/JPHOTOV.2019.2940142.

[6] A. Chaudhary *et al.*, “Influence of Polysilicon Thickness on Properties of Screen-Printed Silver Paste Metallized Silicon Oxide/Polysilicon Passivated Contacts,” *physica status solidi (a)*, vol. 218, no. 18, p. 2100243, 2021, doi: 10.1002/pssa.202100243.

[7] M. Meßmer, “Evaluation of Different Front Surface Passivation Schemes for p-type IBC Solar Cells,” presented at the 15th SiliconPV, 2025.